Available online at www.sciencedirect.com
SCIENCE DIRECT®
Fusion Engineering and Design 73 (2005) 83–93
Fusion Engineering and Design
www.elsevier.com/locate/fusengdes

Code development for analysis of MHD pressure drop reduction in a liquid metal blanket using insulation technique based on a fully developed flow model

Sergey Smolentsev *, Neil Morley, Mohamed Abdou

Department of Mechanical and Aerospace Engineering, UCLA, 44-114 Engineering IV, BOX 951597, Los Angeles, CA 90095-1597, USA

Received 26 November 2004; received in revised form 20 December 2004; accepted 10 January 2005
Available online 24 March 2005

Abstract

The paper presents details of a new numerical code for analysis of a fully developed MHD flow in a channel of a liquid metal blanket using various insulation techniques. The code has specially been designed for channels with a "sandwich" structure of several materials with different physical properties. The code includes a finite-volume formulation, automatically generated Hartmann number sensitive meshes, and effective convergence acceleration technique. Tests performed at $Ha \sim 10^4$ have showed very good accuracy. As an illustration, two blanket flows have been considered: Pb–17Li flow in a channel with a silicon carbide flow channel insert, and Li flow in a channel with insulating coating.

Keywords: Code development; MHD pressure; Insulation technique

1. Introduction

High MHD pressure drop is a crucial point in almost all blanket concepts using liquid metal (Li or Pb–17Li) as a work fluid. The substantial increase in the pressure drop due to MHD effects can be caused by contact of the liquid metal with the electrically conducting channel walls. Unlike the flow in an ideally insulated channel, where all induced currents are closed within the flow domain, in a non-insulated channel, the currents can return through the walls. As a result, the electrical resistance of the wall is a very important parameter that influences the current path and the entire fluid flow. A number of practical approaches have been developed to reduce the MHD pressure drop by insulating the conducting walls. For this purpose, thin ($\sim 10^{-5}$ m) layer coatings have been considered as insulation means in the self-cooled lithium–vanadium blanket [1]. However, fabrication of thin insulating coatings with desirable insulation characteristics is still questionable.

* Corresponding author. Tel.: +1 310 794 5366; fax: +1 310 825 2599.
E-mail address: sergey@fusion.ucla.edu (S. Smolentsev).

0920-3796/$ – see front matter © 2005 Elsevier B.V. All rights reserved.
doi:10.1016/j.fusengdes.2005.01.003

A critical phenomenon that can limit the applicability of such coatings is penetration of liquid metal through the microscopic defects (cracks) in the coating, thus resulting in a direct electrical contact between the liquid and the electrically conducting walls [2–4]. Another potentially attractive approach is based on fabrication of multi-layer coatings [5]. Such coatings consist of several insulator layers "sandwiched" between thin metallic layers. Recently, flow channel inserts (FCI) made of silicon carbide composite (SiC_f/SiC) have been suggested for the electrical and thermal insulation between the liquid breeder and the channel walls [6]. This idea has been implemented in several dual coolant blanket designs with Pb–17Li as a breeder and ferritic steel as a structural material [7–9]. This concept is also being considered as a candidate for blanket tests in ITER [10]. The main advantages of such FCIs is that SiC_f/SiC has relatively low electrical and thermal conductivity, allowing for sufficient reduction of induced electric currents and only insignificant heat escape from the breeder region. As a result, one can expect a relatively low MHD pressure drop and high blanket thermal efficiency. At the same time, the FCI does not serve as a structural element and carries only static (its own weight) and secondary (thermal) stresses, which are expected to be within the allowable limits.

A number of numerical codes for fully developed flows [11–16] have been developed over the last two decades to address some issues related to the MHD pressure drop in liquid metal flows in conducting or insulated channels. The codes differ in using the electric potential [11,12,14,16] or induced magnetic field [13,15] as the main electromagnetic quantity, and utilize either finite-difference [11,13–16] or finite-element [12] methods. They also implement different boundary conditions. The codes based on the induced magnetic field formulation do not often resolve the electromagnetic field in the solid. Instead, "a thin conducting wall boundary condition" [17] is used at the interface between the liquid and solid. Such an approach is generally not applicable to flows in an insulated channel, which typically has a "sandwich" structure of several different materials with different physical properties. Other limitations of the codes include insufficient testing and frequently observed convergence problems at high Hartmann numbers, $Ha \sim 10^3$ to 10^5. The present approach combines the best features of the previous codes and adds new features resulting in an efficient and accurate MHD code that allows for a numerical analysis of the MHD pressure drop, velocity profile and electric current distribution in a liquid metal blanket when using various insulation techniques. The paper describes the numerical method used, mesh generation, and convergence acceleration procedure. The code capabilities are then illustrated with a number of blanket related flows.

2. Formulation

We consider laminar flows of liquid metal through a straight rectangular channel in a transverse (toroidal) strong uniform magnetic field, B_z^0. As an illustration of such a flow, a sketch of the cross-sectional area of the Pb–17Li blanket channel with the SiC_f/SiC FCI is shown in Fig. 1. One can see that the channel wall

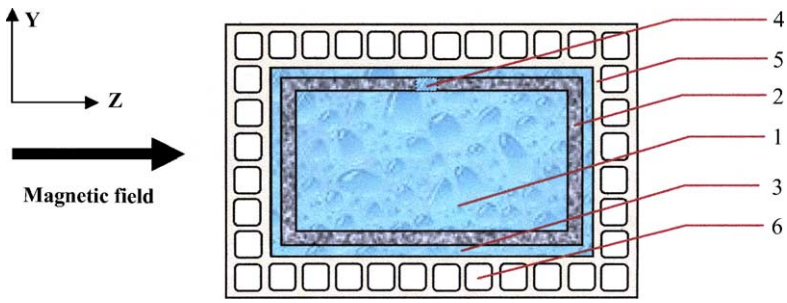

Fig. 1. Sketch of the cross-sectional area of the blanket channel with FCI: (1) Pb–17Li flow in the central channel (0.3 m × 0.2 m); (2) SiC_f/SiC FCI (0.005 m); (3) gap with Pb–17Li (0.002 m); (4) pressure equalization slot (PES) or hole (0.005 m); (5) ferritic wall (0.005 m); (6) cooling channels.

has a typical "sandwich structure". Usually there can be several sub-domains with different physical properties, which can also differ drastically in size. Moreover, the physical properties within a particular sub-domain are not necessarily isotropic. For example electrical and thermal conductivity of SiC_f/SiC composites depends on direction, demonstrating higher values along the fibers. Some of the sub-domains are solid, such as the ferritic wall, FCI or insulating coating. There can also be liquid sub-domains. An example of a liquid sub-domain (additionally to the flow in the central channel) is the flow in the gap between the FCI and the structural ferritic wall. The flow in the gap can be electrically coupled with the flow in the central channel since the SiC_f/SiC insert is not a perfect insulator.

Similar to previous codes, the flows are treated as fully developed. All variables are independent of the axial coordinate x, except for the pressure, P, which is a linear function of x. The problem can be described in terms of the axial velocity, U, and the electric potential, φ. Another possible approach is based on the induced magnetic field, B_x. This choice seems to be more appropriate since some of the previous studies had reported severe convergence problems at high Hartmann numbers when using the φ-formulation [14]. The first author also has results showing some advantages of the B-formulation, especially in the case of non-conducting walls [13]. The governing equations that describe the problem in terms of the velocity and induced magnetic field are [15]:

$$\nu\left(\frac{\partial^2 U}{\partial z^2}+\frac{\partial^2 U}{\partial y^2}\right)-\frac{1}{\rho}\frac{\mathrm{d}P}{\mathrm{d}x}+\frac{1}{\rho}j_y B_z^0=0, \tag{1}$$

$$\frac{1}{\mu_0}\frac{\partial}{\partial z}\left(\frac{1}{\sigma_z}\frac{\partial B_x}{\partial z}\right)+\frac{1}{\mu_0}\frac{\partial}{\partial y}\left(\frac{1}{\sigma_y}\frac{\partial B_x}{\partial y}\right)+B_z^0\frac{\partial U}{\partial z}=0. \tag{2}$$

Providing the induced magnetic field is known, the components of the electric current density vector entering the Lorentz force term in the momentum equation can be calculated as

$$j_y=\frac{1}{\mu_0}\frac{\partial B_x}{\partial z},\qquad j_z=-\frac{1}{\mu_0}\frac{\partial B_x}{\partial y}. \tag{3}$$

Here μ_0 is the magnetic permeability of vacuum, ν the kinematic viscosity, ρ the density, and σ the electrical conductivity. The notations σ_x and σ_y are introduced to show anisotropy in σ. Generally, the electrical conductivity is a discontinuous function of the coordinates. For example, the electrical conductivity of SiC is four orders of magnitude lower than that of liquid metal. In the code, the momentum equation (1) is solved in the liquid only, while the induction equation (2) is integrated over the whole domain, including all liquid and solid sub-domains. The boundary condition on the velocity is a no-slip condition at the interface between the liquid and solid. The external boundary condition on B_x provides no induced magnetic field at the outer boundary of the integration domain. The internal boundary conditions can also be formulated at the inner interfaces between the sub-domains with different physical properties. However, in the present code the internal boundary conditions are not used. Instead, the conservative properties are provided through the conservation form of the induction equation (σ is inside the derivative). This also allows continuous integration of the induction equation over the whole domain without iterating between solutions in different sub-domains.

It is more convenient to rewrite Eqs. (1) and (2) in a dimensionless form by using proper scales: $[z]=[y]=b$ is a length scale (b is the half of the flow dimension in the direction of the applied magnetic field); $[U]=b^2\nu^{-1}\rho^{-1}(-\mathrm{d}p/\mathrm{d}x)$ is a velocity scale; and $[B_x]=b^2\mu_0(\sigma/\nu\rho)^{0.5}(-\mathrm{d}p/\mathrm{d}x)$ is a scale for the induced magnetic field. The equations can then be written as follows:

$$\frac{\partial^2 U}{\partial z^2}+\frac{\partial^2 U}{\partial y^2}+1+Ha\frac{\partial B}{\partial z}=0, \tag{4}$$

$$\frac{\partial}{\partial z}\left(\bar{\sigma}_z\frac{\partial B}{\partial z}\right)+\frac{\partial}{\partial y}\left(\bar{\sigma}_y\frac{\partial B}{\partial y}\right)+Ha\frac{\partial U}{\partial z}=0. \tag{5}$$

Here B denotes the dimensionless induced magnetic field, while the same notations are used for the dimensionless velocity and coordinates. The Hartmann number is built through the dimension b: $Ha=B_z^0 b(\sigma/\nu\rho)^{0.5}$. The dimensionless parameter $\bar{\sigma}$ is the ratio of the electrical conductivity of liquid to its local value.

3. Numerical method and computer code

3.1. Numerical scheme

A classic (rectangular) shape of the integration domain is a major factor that dictates the choice of a numerical method. Due to the relatively simple geometry there is no direct need for using boundary fitted coordinates or a finite-element method. Instead, a control-volume technique based on non-uniform collocated Cartesian meshes can be used, giving a reasonably simple but a pretty accurate approach. Both the velocity and magnetic field are defined at the center of the control-volume cell, while the fluxes are defined at the center of the cell side. The approximations of Eqs. (4) and (5) were then constructed using the finite-volume formulation in the following form:

$$\frac{U^{n+1}_{i,j}-U^{n}_{i,j}}{\Delta t}=\frac{[(U^{n+1}_{i+1,j}-U^{n+1}_{i,j})/(z_{i+1}-z_i)]-[(U^{n+1}_{i,j}-U^{n+1}_{i-1,j})/(z_i-z_{i-1})]}{0.5(z_{i+1}-z_{i-1})}+\frac{[(U^{n+1}_{i,j+1}-U^{n+1}_{i,j})/(y_{j+1}-y_j)]-[(U^{n+1}_{i,j}-U^{n+1}_{i,j-1})/(y_j-y_{j-1})]}{0.5(y_{j+1}-y_{j-1})}+Ha\frac{B^{n}_{i+1,j}-B^{n}_{i-1,j}}{z_{i+1}-z_{i-1}}+1, \tag{6}$$

$$\frac{B^{n+1}_{i,j}-B^{n}_{i,j}}{\Delta t}=\frac{\bar{\sigma}_{i+1/2,j}[(B^{n+1}_{i+1,j}-B^{n+1}_{i,j})/(z_{i+1}-z_i)]-\bar{\sigma}_{i-1/2,j}[(B^{n+1}_{i,j}-B^{n+1}_{i-1,j})/(z_i-z_{i-1})]}{0.5(z_{i+1}-z_{i-1})}+\frac{\bar{\sigma}_{i,j+1/2}[(B^{n+1}_{i,j+1}-B^{n+1}_{i,j})/(y_{j+1}-y_j)]-\bar{\sigma}_{i,j-1/2}[(B^{n+1}_{i,j}-B^{n+1}_{i,j-1})/(y_j-y_{j-1})]}{0.5(y_{j+1}-y_{j-1})}+Ha\frac{U^{n}_{i+1,j}-U^{n}_{i-1,j}}{z_{i+1}-z_{i-1}}, \tag{7}$$

where the effective $\bar{\sigma}$ is taken at the sides of the control-volume cell. Although the electrical conductivity is a discontinuous function of the coordinates, approximation (7) reproduces the conservation law embedded in the induction equation [18]. Eqs. (6) and (7) include an additional pseudo-time term, which is not present in the original equations. The steady-state solution independent of t is sought by a relaxation technique.

3.2. Computational mesh

Special attention has been paid to the mesh construction. Such a mesh should take into account high velocity and magnetic field gradients in the flow. The mesh should also properly resolve the induced magnetic field in the thin solid layers, such as the insulating coating, and within the microscopic cracks. A special feature of the flows considered is the formation of thin Hartmann layers ($\sim 1/Ha$) at the channel walls perpendicular to the magnetic field, and secondary (side) layers ($\sim 1/Ha^{0.5}$) at the walls parallel to the magnetic field. The Hartmann layers appear not only in the flow in the central channel but also in the gap between the FCI and the ferritic wall and in other liquid sub-domains. As previous calculations showed, for reasonable accuracy it is necessary to have at least 7–10 mesh points within the Hartmann layers. These requirements at high $Ha \sim 10^3$ to 10^5 are very severe and can be satisfied with only special non-uniform meshes, which cluster the points in the gradient regions and provide smaller mesh spacing near the walls at higher Ha. Similar to [13], such meshes were generated in the present code with the following stretching transformation [19]:

$$s = h\frac{(\beta+2\alpha)[(\beta+1)/(\beta-1)]^{(\bar{s}-\alpha)/(1-\alpha)}-\beta+2\alpha}{(2\alpha+1)\{1+[(\beta+1)/(\beta-1)]^{(\bar{s}-\alpha)/(1-\alpha)}\}}. \tag{8}$$

With this formula a uniform mesh $\bar{s}_k$ ($0 \le \bar{s}_k \le 1$) can be transformed into a refined mesh s_k ($0 \le s_k \le h$). If $\alpha = 0$, the mesh will be refined near $s = h$ only, whereas if $\alpha = 0.5$, the mesh will be refined equally near $s = 0$ and $s = h$. The stretching parameter β is related to the non-dimensionless boundary-layer thickness (δ/h) by $\beta = (1-\delta/h)^{-0.5}$. In terms of the Hartmann number the

last formula can be modified as follows:

$$\beta = \begin{cases} \left[\dfrac{Ha}{Ha-1}\right]^{0.5} & \text{(to resolve Hartmann layers)}, \\ \left[\dfrac{\sqrt{Ha}}{\sqrt{Ha}-1}\right]^{0.5} & \text{(to resolve side layers)}. \end{cases} \tag{9}$$

Another transformation used in the code that refines the mesh about some interior point s_c is given by the following equation [20]:

$$s = s_c \left\{1 + \frac{\sin h[\tau(\bar{s}-\gamma)]}{\sin\, h(\tau\gamma)}\right\}. \tag{10}$$

In this formula, τ is the stretching parameter, which varies from zero (no stretching) to large values that produce the most refinement near $s = s_c$. The parameter γ is related to τ by

$$\gamma = \frac{1}{2\tau} \ln\left[\frac{1 + (e^{\tau} - 1)(s_c/h)}{1 + (e^{-\tau} - 1)(s_c/h)}\right].$$

Transformation (10) is used for refining the mesh in and around a crack in the insulating coating or within the pressure equalization slot in the FCI.

3.3. Code

The code is written in Fortran. First, the code reads the input data, such as a number of sub-domains, their dimensions, physical properties, a number of mesh points for each sub-domain, pseudo-time step, and convergence criteria. Then, the Hartmann numbers and the stretching parameters β are calculated for each liquid sub-domain. After that, the code generates a non-uniform mesh in the liquid, and in the solid sub-domains using coordinate transformation (8). The stretching parameters in the liquid are calculated using formulas (9), while those in the solid sub-domains are adjusted to provide the same mesh spacing on both sides of the liquid–solid or solid–solid interface. As a result, the generated grid refines the mesh points in the gradient layers in the liquid and at the interfaces. At the same time the mesh sizes at the interfaces do not differ significantly even though the two sub-domains on both sides from the interface have dimensions that differ by orders of magnitude. In problems with the pressure equalization slot or cracks in the insulating coating, the mesh is also refined using formula (10). The stretching parameter τ is adjusted to have sufficiently fine meshes in the crack or PES area. An example of a refined mesh is shown in Fig. 2.

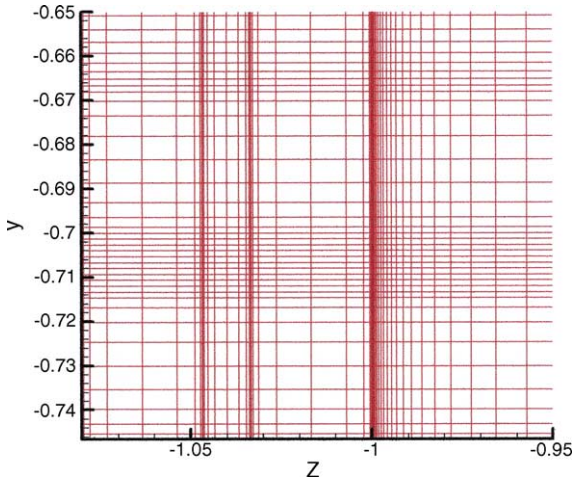

Fig. 2. Example of a computational mesh generated for a blanket channel with FCI at $Ha = 1000$. The mesh is refined near the interfaces. Only corner region of about 1/200 of the whole domain is shown. More clustering is in the Z-direction to resolve the Hartmann layers.

The code solves finite-difference equations (6) and (7) using Alternative Direction Implicit (ADI) method [21]. Eq. (6) is solved in the liquid sub-domains only. First, the passes are performed in the OZ direction in the gaps (if any), and then in the central duct and PES. Then, the passes are performed in the OY direction in the same order. However the sequence, in which passes are performed, does not have a significant effect on the code efficiency and is chosen for reasons of a more compact code. Eq. (7) is solved over the whole domain. A special relaxation technique is used to accelerate convergence (see details in Section 3.4). Applying this technique is especially effective at high Hartmann numbers ($\sim 10^4$) when the number of iterations reaches 10^5 to 10^6 and the computations take many hours. After finishing the iteration, a dimensionless volumetric flow rate Q is calculated in each liquid sub-domain by integrating numerically the velocity distribution:

$$Q = \int\int U(z, y)\, \mathrm{d}z\, \mathrm{d}y. \tag{11}$$

The dimensionless flow rate in the central channel flow is related to the dimensional pressure gradient with the

following formula:

$$-\frac{\mathrm{d}P}{\mathrm{d}x} = \frac{4U_{\mathrm{m}}\nu\rho}{b^2\chi Q}. \tag{12}$$

Here U_{m} is the mean velocity in the central channel, and $\chi = b/h$ the channel aspect ratio. The computations are finished when the condition $|(Q^{n+1} - Q^n)/Q^{n+1}| < \varepsilon$ is repeated many times in each liquid sub-domain. Usually the number of the repetitions is $Nr = 500$–5000. The convergence criterion is $\varepsilon = 10^{-10}$ to 10^{-7}. Bigger Nr and smaller ε are used at higher Ha. All computations presented in the paper were performed using a PC (Intel Pentium 4, 2.26 GHz) with double precision.

3.4. Acceleration of convergence

Solving Eqs. (6) and (7) independently with the ADI technique with a fixed source term on the RHS does not apply any limitations on the integration time step. However when solving (6) and (7) together, the time step should be small enough to avoid oscillations in the solution that may appear due to the excessively high changes in the source term. The limitations on the time step become especially severe at high Hartmann numbers that make the computations unacceptably long. For example, at $Ha = 15{,}000$, $\Delta t \sim 10^{-8}$, which requires several days of calculations. Thus, implementing a technique that could accelerate convergence at high Ha becomes important.

An example of convergence is shown in Fig. 3 for a rectangular channel with conducting or perfectly insulated walls. The case of conducting wall assumes two conducting Hartmann and two non-conducting side walls. One can see that the case of electrically conducting walls requires much more iterations, and the flow rate oscillates before the steady-state solution is achieved. When the flow rate changes the sign, the velocity and the induced currents reverse their direction. One idea for accelerating convergence in the case of electrically conducting channel walls is then to apply a kind of relaxation technique:

$$\tilde{U}_{i,j} = U^{n\,\min}_{i,j} + \omega(U^{n\,\max}_{i,j} - U^{n\,\min}_{i,j}),$$
$$\tilde{B}_{i,j} = B^{n\,\min}_{i,j} + \omega(B^{n\,\max}_{i,j} - B^{n\,\min}_{i,j}). \tag{13}$$

Here $\tilde{U}$ and $\tilde{B}$ are corrected values, and ω a relaxation parameter. Two velocity distributions, $U^{n\,\min}$ and $U^{n\,\max}$, and two induced magnetic field distributions, $B^{n\,\min}$ and $B^{n\,\max}$, involved in the relaxation procedure, are taken from two different iteration levels, $n\,\min$ and $n\,\max$, that correspond to the local minimum and maximum of the volumetric flow rate. The relaxation procedure is applied each time when $(Q^n - Q^{n-1})(Q^{n+1} - Q^n)$ becomes negative. Thus, the present technique is different from the standard under- or over-relaxation procedure, which is applied successively. The best convergence rate for electrically conducting walls has been found at $\omega = 0.5$. Using the relaxation procedure at high Hartmann numbers can reduce the number of iterations by more than one order. It also allows for a slightly bigger integration time step. The tendency of reducing the number of iteration, by using the relaxation procedure can be seen in Fig. 3 and is also illustrated in Table 1.

4. Testing the code

First, a configuration was generated that corresponds to the case treated by Hunt [22]. In Hunt's problem, two walls perpendicular to the magnetic field (Hartmann walls) are treated as conducting, and two

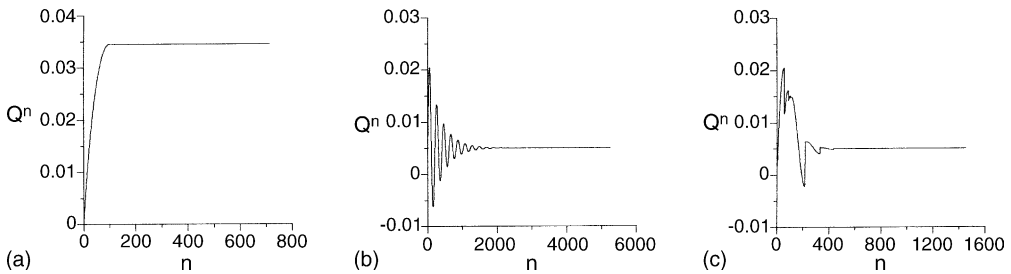

Fig. 3. Volumetric flow rate in a rectangular channel at $Ha = 100$ as a function of the iteration number, n, calculated for perfectly insulated (a) and conducting (b and c) walls with (c) and without (a and b) the relaxation.

Table 1
Number of iterations, NIT, with and without relaxation, for a channel with electrically conducting walls

Ha	Δt	NIT (without relaxation)	NIT (with relaxation)
100	0.2×10^{-3}	5248	1454
200	0.5×10^{-4}	17284	2261
500	0.1×10^{-4}	59038	4761
1000	0.3×10^{-5}	132877	10272

Number of grid points in the flow domain and across the wall is 101×101 and 45. Other parameters are: $\varepsilon = 10^{-7}$; $Nr = 500$.

other walls (side walls) as non-conducting. We will refer to this case as test case 1. There can be some differences between the data computed by the present code and Hunt's analytical solution, since in the analytical approach "thin conducting wall boundary conditions" [17] were used, while the present code calculates the whole domain including the walls. To meet the thin conducting wall conditions, we used $t_w/b = 0.008$. Three dimensionless parameters entering Hunt's solution are the Hartmann number, the channel aspect ratio, and the wall conductance ratio, defined here as $c_w = t_w\sigma_w/b\sigma$, The results for the Hartmann number, 1000 and 10,000, and two conductance ratios, 0 and 0.016, are summarized in Table 2. The comparison demonstrates very good computational accuracy. Velocity distributions calculated with the code are shown in Fig. 4. Table 3 illustrates sensitivity of the volumetric flow rate calculated with the code to the computational mesh.

A number of qualitative tests were also performed to validate the code in the case of more than two subdomains. First, the calculations were conducted for the channel shown in Fig. 1 without a magnetic field (test case 2). The velocity distributions (Fig. 5) are qualitatively correct, demonstrating a dome-type velocity profile in the central channel and a parabolic distribution in the gap. In the next test, a magnetic field was applied but the electrical conductivity of the FCI and that of the structural wall were taken very small (test case 3). As expected, classic MHD velocity profile was obtained in the central channel with a uniform flow in the core, two Hartmann, and two side layers (Fig. 6). At the same time the flow in the left and right gaps is typical Hartmann flow (except for the corner regions).

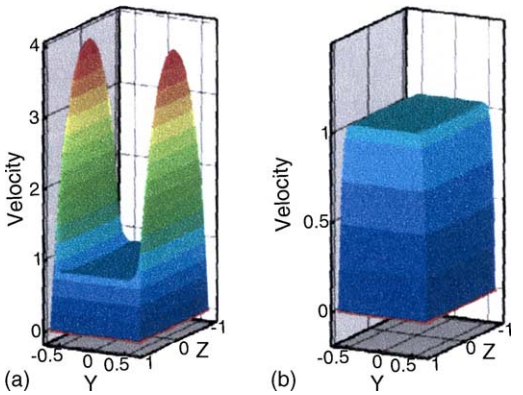

Fig. 4. Test case 1. Flow in a rectangular channel at $Ha = 1000$, $\chi = 1.5$: (a) conducting Hartmann walls ($c_w = 0.016$); (b) all walls non-conducting.

Table 3
Test case 1: sensitivity of the volumetric flow rate calculated with the code to the computational mesh

Mesh	Q (Code)	Q (Hunt)
$Ha = 1000$, $c_w = 0$		
101×101, 45	0.3833×10^{-2}	0.3833×10^{-2}
75×75, 21	0.3825×10^{-2}	0.3833×10^{-2}
45×45, 15	0.3790×10^{-2}	0.3833×10^{-2}
$Ha = 1000$, $c_w = 0.016$		
101×101, 45	0.2878×10^{-3}	0.2875×10^{-3}
75×75, 21	0.2879×10^{-3}	0.2875×10^{-3}
45×45, 15	0.2882×10^{-3}	0.2875×10^{-3}

Table 2
Test case 1: comparison between the calculations by the present code and the analytical solution for a flow in a rectangular channel ($\chi = 1.5$) with conducting Hartmann and non-conducting side walls

Ha	c_w	Δt	NIT	Time (min)	Q (Hunt)	Q (Code)
1000	0	0.4×10^{-5}	8114	12	0.3833×10^{-2}	0.3833×10^{-2}
1000	0.016	0.4×10^{-5}	11061	17	0.2875×10^{-3}	0.2878×10^{-3}
10000	0	0.5×10^{-7}	24439	38	0.3947×10^{-3}	0.3947×10^{-3}
10000	0.016	0.5×10^{-7}	53746	82	0.4291×10^{-5}	0.4301×10^{-3}

The computational mesh includes 101×101 points in the flow domain and 45 points across the wall; $\varepsilon = 10^{-8}$, $Nr = 5000$.

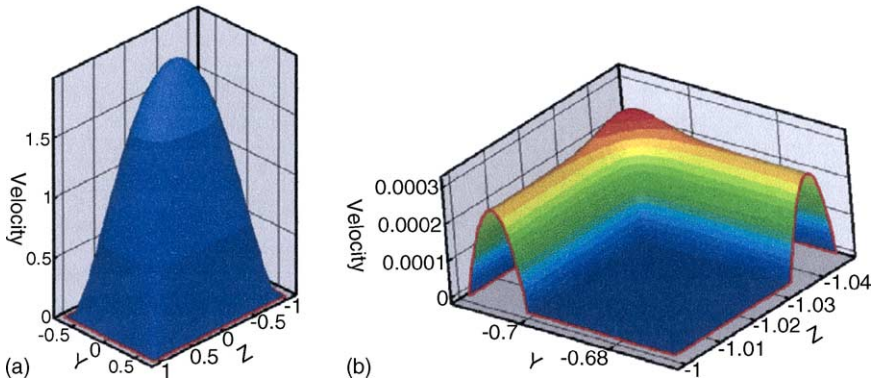

Fig. 5. Test case 2. Flow without a magnetic field in the channel shown in Fig. 1: velocity in the central channel (a), and in the corner gap (b). All velocities are scaled by the mean velocity in the central channel.

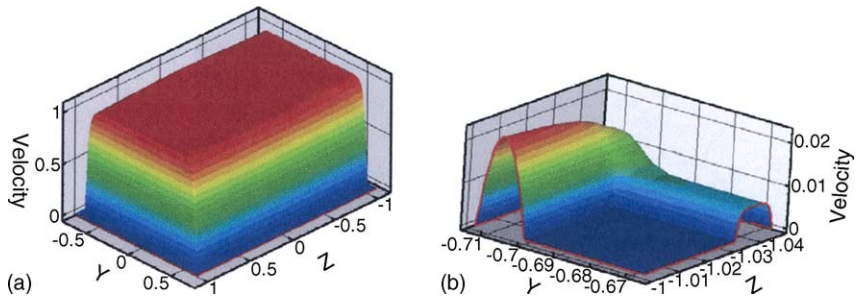

Fig. 6. Test case 3. Flow in the channel shown in Fig. 1 with all solids non-conducting at $Ha = 1000$: velocity in the central channel (a), and in the corner gap (b).

The flows in the two other gaps are parabolic since the magnetic field is parallel to the long side of the gap, and thus the field almost does not affect the flow.

5. Examples

5.1. Pb–17Li flow in a blanket channel with SiC_f/SiC FCI

The idea of using SiC FCI as electrical/thermal insulator in a PbLi blanket was first formulated in [7]. Here, we use basic dimensions shown in Fig. 1 as was recently suggested for the dual coolant Li–17Pb US DEMO blanket [9]. There can be two types of pressure equalization openings in the FCI: an axial pressure equalization slot or a number of pressure equalization holes placed in line some distance apart in the axial direction at one of the FCI sides. Both types serve the same goal: to make the pressure on both sides of the FCI equal, thus eliminating the primary stress. The latter variant was adopted in the present calculation. The calculations were performed for the channel section between two pressure equalization holes, assuming a fully developed flow there. The electrical conductivity of SiC_f/SiC depends on the fabrication technique and can vary in a wide range. The value used in the calculations was 500 $\Omega^{-1}\,m^{-1}$ as recommended in [23]. No anisotropy in σ was introduced. The electrical conductivity of the ferritic wall and Pb–17Li is 1.4×10^6 and $0.7 \times 10^6\,\Omega^{-1}\,m^{-1}$ correspondingly. The dynamic viscosity of Pb–17Li is 0.001 Pa s. The applied magnetic field is 4 T. The Hartmann number calculated for the flow in the central channel is 15,875, and that in the flow through the left or right gap is 106. The computational mesh includes 101×101 points in the central channel, 15 points both across the ferritic wall and the FCI, and 27 across the gap. The computational time

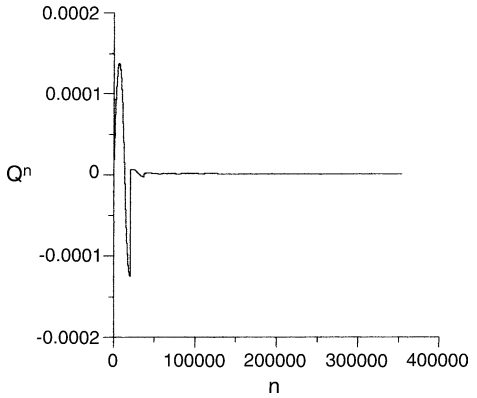

Fig. 7. Convergence in the calculations of Pb–17Li flow in a blanket channel with FCI using the relaxation procedure.

step is 1.0×10^{-8}. The convergence parameters are: $\varepsilon = 10^{-9}$, and $Nr = 5000$. The time independent solution was achieved for 353,900 iterations. The calculations took almost 12 h using relaxation. The convergence is illustrated in Fig. 7. The mass flow rate shown in this figure tends to a very small but positive value.

The velocity and induced magnetic field distributions are shown in Fig. 8. Fig. 8a shows the velocity profile both in the central channel and in the gap. Fig. 8c gives an enlarged view of the velocity distribution in the gap. The velocity profile in the central channel demonstrates high velocity jets and a stagnant core. The velocity in the left (right) gap is low, about 0.2, while it is extremely high in the bottom (top) gap, reaching the same value of about 8 at the midplane as the jet velocity in the central channel. The dimensionless flow rate in the central channel is $Q = 0.1308 \times 10^{-5}$. It is considerably lower than that in a perfectly insulated channel ($Q = 0.2494 \times 10^{-3}$), but about one order of magnitude higher than that in a channel with bare walls ($Q = 0.1618 \times 10^{-6}$). The latter was calculated using an asymptotic formula valid at high *Ha*: $-\mathrm{d}P/\mathrm{d}x = \sigma U_m B_z^{0^2} c_\mathrm{w}/(1 + c_\mathrm{w})$, which after combining with Eq. (12) gives

$$Q = \frac{4\nu\rho}{b^2 \chi \sigma B_z^{0^2}} \frac{1 + c_\mathrm{w}}{c_\mathrm{w}}.$$

It should be noted that the present calculations just illustrate the code applicability. To judge feasibility of a particular blanket design with FCI, one should choose a type of pressure equalization opening; optimize their location and size; and quantify the impact of the MHD results on the MHD pressure drop and temperature distribution in the blanket.

5.2. Li flow in a coated channel with cracks

Calculations were performed for a slotted channel with the aspect ratio $\chi = 5$ ($b = 0.05$ m) in a 5 T magnetic field parallel to the longer side of the channel. The computational domain consists of the fluid, solid wall ($t_\mathrm{w} = 0.002$ m) and insulating coating between them ($t_\mathrm{c} = 50$ μm). The electrical conductivity of the liquid is $2.8\ \Omega^{-1}\ \mathrm{m}^{-1}$, and that of the wall is two times smaller. The Hartmann number is then 20,000. The ratio of the electrical conductivity in the liquid to that of the insulating coating was assumed to be 10^9. This value guarantees ideal insulation, providing no defects in the coating

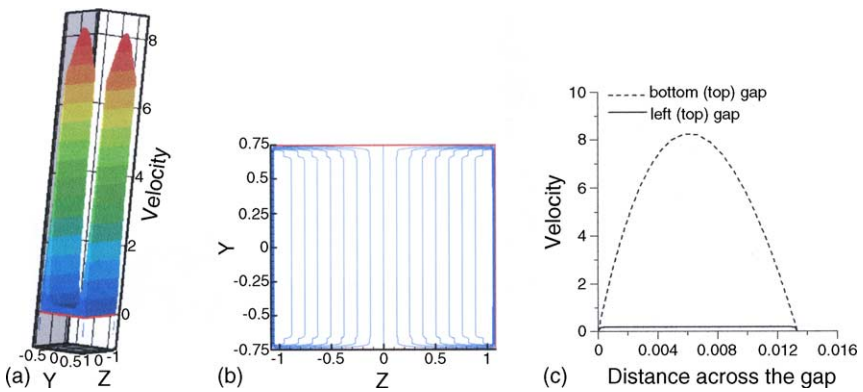

Fig. 8. Flow in a blanket channel with FCI: velocity profile (a), induced magnetic field (b), velocity distribution in the gaps (c). All velocities are scaled by the mean velocity in the central channel.

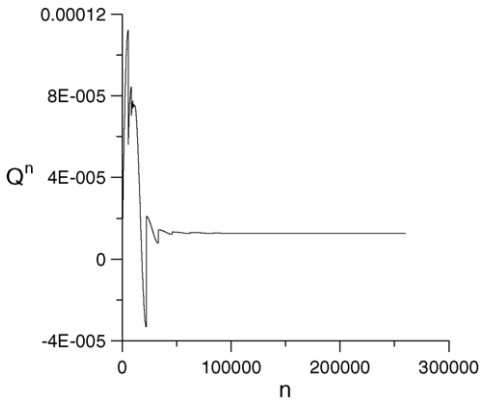

Fig. 9. Convergence in the calculations of Li flow in a blanket channel with insulating coating and two corner cracks. No relaxation was applied.

appear. Two microscopic cracks in the coating, 5 μm each, are located at the left top and right bottom corners. The computational mesh includes 101 × 101 points in the flow domain and 13 points across both the wall and the insulating coating. The crack area is resolved with 7 × 13 mesh points. The time step is 1.0×10^{-8}. The convergence parameters are: $\varepsilon = 10^{-10}$, and $Nr = 5000$. No relaxation was applied. The computations took 6 h. The convergence curve is shown in Fig. 9.

The electric currents generated in the flow leave the flow domain through one of the cracks, then flow through the electrically conducting wall and return back in the flow domain through the other crack. The electric current streamlines in the crack area are shown in Fig. 10. The dimensionless flow rate in the case with the cracks is 0.1272×10^{-4}, while it is 0.1940×10^{-3} if there are no cracks. Therefore, in the reference case,

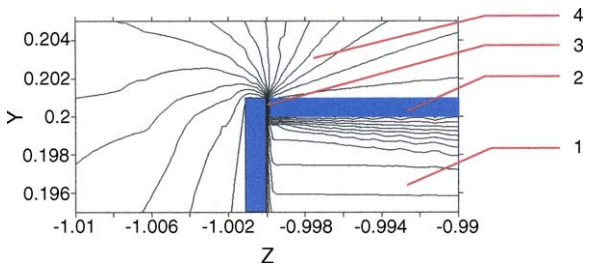

Fig. 10. Induced electric current distribution in the left top crack area in a Li blanket channel with insulating coating: (1) liquid; (2) insulating coating (50 μm); (3) corner crack (5 μm); (4) wall.

two microscopic corner cracks result in an MHD pressure drop increase of almost one order of magnitude.

6. Conclusions

A finite-difference computer code has been developed for a fully developed MHD flow under fusion reactor blanket conditions. The code can be applied to typical liquid metal flows in a single blanket channel or a group of electrically connected channels, with or without insulation. Possible flow configurations include a lithium–vanadium blanket with mono- or multilayer insulating coatings, and Pb–17Li blanket with a silicon carbide flow channel insert. The distinctive features of the code include a finite-volume formulation, automatically generated Hartmann number sensitive meshes, and effective convergence acceleration technique. The code was verified against the analytical solutions. The comparisons have demonstrated a very good accuracy even at very high Hartmann numbers ($\sim 10^4$) for both conducting and non-conducting walls. As an example, two MHD flows have been calculated: Pb–17Li flow in a blanket channel with a silicon carbide flow channel insert, and Li flow in a blanket channel with insulating coating with or without cracks. Typical calculation time under blanket conditions is about 10 h using a PC.

Acknowledgement

The authors would like to express their gratitude to Drs. Clement Wong, Siegfried Malang, and Igor Kirillov for their valuable comments and suggestions.

References

[1] D.L. Smith, J.-H. Park, I. Lyublinski, V. Evtikhin, A. Perujo, H. Glassbrenner, T. Terai, S. Zinkle, Progress in coating development for fusion systems, Fusion Eng. Des. 61/62 (2002) 629–641.
[2] A. Ying, A. Gaizer, The effects of imperfect insulating coatings on MHD and heat transfer in rectangular ducts, Fusion Eng. Des. 27 (1995) 634–641.
[3] L. Buhler, The influence of small cracks in insulating coatings on the flow structure and pressure drop in MHD channel flows, Fusion Eng. Des. 27 (1995) 650–658.

[4] S. Malang, L. Buhler, MHD pressure drop in ducts with imperfectly insulating coatings, ANL/FPP/TM-269, 1994.
[5] I.R. Kirillov, RF DEMO team, lithium cooled blanket of RF DEMO reactor, Fusion Eng. Des. 49/50 (2000) 457–465.
[6] M.S. Tillack, S. Malang, High performance PbLi blanket, in: Proceedings of the 17th IEE/NPSS Symposium on Fusion Engineering, vol. 2, San Diego, CA, October 6–10, 1997, pp. 1000–1004.
[7] ARIES TeamM.S. Tillack, X.R. Wang, J. Pulsifer, S. Malang, D.K. Sze, ARIES-ST breeding blanket design and analysis, Fusion Eng. Des. 49/50 (2000) 689–695.
[8] P. Norajitra, L. Buhler, U. Fisher, S. Malang, G. Reinmann, H. Schnauder, The EU advanced dual coolant blanket concept, Fusion Eng. Des. 61/62 (2002) 449–453.
[9] C. Wong, S. Malang, M. Sawan, S. Smolentsev, S. Majumdar, B. Merrill, D.K. Sze, N. Morley, S. Sharafat, P. Fogarty, M. Dagher, P. Peterson, H. Zhao, S. Zinkle, M. Youssef, Assessment of liquid breeder first wall and blanket options for the DEMO design, in: Proceedings of the 16th ANS TOFE Meeting, Madison, September 14–16, 2004.
[10] M. Abdou, D. Sze, C. Wong, M. Sawan, A. Ying, N. Morley, US plans and strategy for ITER blanket testing, in: Proceedings of the 16th ANS TOFE Meeting, Madison, September 14–16, 2004.
[11] A. Sterl, Numerical simulation of liquid-metal MHD flows in rectangular ducts, J. Fluid Mech. 216 (1990) 161–191.
[12] M. Tillack, A. Ying, H. Hashizume, The effect of magnetic field alignment on heat transfer in liquid metal blanket channels, UCLA-FNT-24, March 1989.
[13] S. Smolentsev, A. Tananaev, Development of computer code for analysis of heat transfer in liquid metal MHD flows in ducts, in: Proceedings of the Second International PAMIR Conference on Energy Transfer in Magnetohydrodynamic Flows, vol. 2, Aussois, France, 1994, pp. 551–560.
[14] H. Araseki, S. Kotake, A self-correcting procedure for computational liquid metal magnetohydrodynamics, J. Comput. Phys. 110 (1994) 301–309.
[15] S. Smolentsev, Mathematical models for magnetohydrodynamic flows in a fusion reactor blanket, Plasma Dev. Oper. 7 (1999) 231–241.
[16] N. Umeda, M. Takahashi, Numerical analysis for heat transfer enhancement of a lithium flow under a transverse magnetic field, Fusion Eng. Des. 51/52 (2000) 899–907.
[17] J.S. Walker, Magnetohydrodynamic flows in rectangular ducts with thin conducting walls, J. Mec. 20 (1981) 79–112.
[18] R.J. MacKinnon, G.F. Carey, Analysis of material interface discontinuities and superconvergent fluxes in finite difference theory, J. Comput. Phys. 75 (1988) 151–167.
[19] G.O. Roberts, Computational meshes for boundary layer problems, in: Proceedings of the Second International Conference on Numerical Methods Fluid Dynamics, Lecture Notes on Physics, vol. 8, Springer-Verlag, New York, 1971, pp. 171–177.
[20] J.C. Tannehill, D.A. Anderson, R.H. Pletcher, Computational Fluid Mechanics and Heat Transfer, 2nd ed., Taylor & Francis, 1997.
[21] D.W. Peaceman, H.H. Rachford, The numerical solution of parabolic and elliptic differential equations, J. Soc. Ind. Appl. Math. 3 (1955) 28–41.
[22] J.C.R. Hunt, Magnetohydrodynamic flow in rectangular ducts, J. Fluid Mech. 21 (1965) 577–590.
[23] A.R. Raffray, R. Jones, G. Aiello, M. Billone, L. Giancarli, H. Golfier, A. Hasegawa, Y. Katoh, A. Kohyama, S. Nishio, B. Riccardi, M.S. Tillack, Design and material issues for high performance SiC_f/SiC-based fusion power cores, Fusion Eng. Des. 55 (2001) 55–95.